

Antiferromagnetic interlayer coupling in ferromagnetic semiconductor EuS/PbS(001) superlattices

H. KEPA^{1,6}(*), J. KUTNER-PIELASZEK¹, J. BLINOWSKI¹, A. TWARDOWSKI¹, C.F. MAJKRZAK², T. STORY³, P. KACMAN³, R.R. GALAŻKA³, K. HA⁴, H.J.M. SWAGTEN⁴, W.J.M. DE JONGE⁴, A.YU. SIPATOV⁵, V. VOLOBUEV⁵ and T.M. GIEBULTOWICZ⁶

¹ *Department of Physics, Warsaw University – ul. Hoża 69, 00-681 Warszawa, Poland*

² *National Institute of Standards and Technology – Gaithersburg, MD 20899, USA*

³ *Institute of Physics, Polish Academy of Sciences – Al. Lotników 32/46, 02-668 Warszawa, Poland*

⁴ *Department of Applied Physics and COBRA – Eindhoven University of Technology, 5600 MB Eindhoven, The Netherlands*

⁵ *Kharkov State Polytechnical University – 21 Frunze St., 310002 Kharkov, Ukraine*

⁶ *Physics Department, Oregon State University – Corvallis, OR 97331, USA*

PACS. 61.12Ha – Neutron reflectometry.

PACS. 68.65Cd – Superlattices.

PACS. 75.50Pp – Magnetic semiconductors.

Abstract. – Antiferromagnetic coupling between ferromagnetic layers has been observed for the first time in an all-semiconductor superlattice structure EuS/PbS(001), by neutron scattering and magnetization measurements. Spin-dependent superlattice band structure effects are invoked to explain the possible origin and the strength of the observed coupling.

Since the discovery of antiferromagnetic (AFM) coupling between metallic ferromagnetic (FM) layers separated by a nonmagnetic metal in late 1980s, the subject has been an active research area in fundamental magnetism. The AFM coupling plays a key role in many technological applications such as magnetoresistive sensors and magneto-optical devices [1]. In metallic systems, the interlayer coupling results from the quantum interference of conduction electron waves in the spin dependent potential of magnetic multilayer or, equivalently, via the spin polarization of conducting carriers (an analog of the well-known RKKY interaction [2, 3]). An important question arises as to how interlayer coupling can exist in non-metallic systems. Recently, efforts have been made to study the interlayer coupling in hybrid systems composed of metallic ferromagnets separated by semiconductor layers. In particular, Fe/Si trilayers and multilayers had attracted much attention, but the coupling turned out to proceed via metallic iron silicide, and not via the silicon, due to intermixing between iron and silicon occurring even at room temperature [4]. This is one illustration of the severe limitations brought about by the technological incompatibility of FM metals and semiconductors. There is no such limitation in the case of the magnetic/nonmagnetic multilayers composed of properly chosen

(*) E-mail: Henryk.Kepa@fuw.edu.pl

all-semiconductor materials. By means of neutron diffraction, an interlayer exchange interaction was observed in *semiconductor antiferromagnetic/nonmagnetic* EuTe/PbTe, MnTe/ZnTe and MnTe/CdTe superlattices (SLs) [5–7]. The *ferromagnetic/nonmagnetic semiconductor* GaMnAs/AlGaAs system [8] was also studied where a *ferromagnetic* interlayer exchange was detected in magnetic hysteresis measurements. Here the coupling is believed to be mediated, as in metals, by conducting carriers (holes) in the nonmagnetic layer, though the very origin of ferromagnetism in GaMnAs [9, 10] is an on-going debate. Recently developed models of interlayer coupling specific to the FM semiconductor multilayers, considered in [11–13], lead also to the FM correlations.

In this Letter, we present the first conclusive evidence for the existence of AFM interlayer coupling in all-semiconductor ferromagnet/diamagnet EuS/PbS(001) multilayers, based on neutron diffraction, neutron reflectivity, and magnetization measurements. AFM correlations in EuS/PbS multilayers are seen for PbS thickness up to 90 Å. Since AFM interlayer coupling is a crucial element for the operation of many important magnetic thin film structures, such as spin valves, the present finding is of potential technological as well as fundamental scientific interest.

Although many samples with different EuS and PbS thicknesses (30Å– 80Å and 4Å– 90Å, respectively) have been examined for this study, we will focus on the results of three representative samples, which we shall label as samples I, II, and III. The compositions of the samples are [30Å EuS/4.5Å PbS]×20, [35Å EuS/10Å PbS]×10, and [60Å EuS/23Å PbS]×15 respectively. EuS and PbS are semiconducting materials which crystallize in the rocksalt structure with a lattice mismatch of about 0.5%. EuS is a well-known nonmetallic (semi-insulating) Heisenberg ferromagnet. PbS is a diamagnet with a narrow band gap; its carrier concentration is typically of the order of 10^{17} to 10^{18} cm⁻³. The multilayers were grown epitaxially on monocrystalline KCl(001) substrate and several hundred angstroms thick PbS buffer using electron beam for EuS evaporation and standard resistive heating for PbS evaporation. The quality of the SLs was examined by X-ray and neutron diffraction. Figure 1(a) shows X-ray reflectivity profiles for the samples III and I. Four order of SL Bragg peaks are visible for the sample III, and two order are shown for the sample I, the latter one having much smaller SL periodicity. In Figure 1(b) high angle diffraction spectra for the sample II and again the sample I are presented. Large number of SL satellites visible in both cases clearly indicates the high degree of the superlattice structural perfection. Detailed studies of the growth and magnetic properties of EuS/PbS multilayers with thick PbS spacers (magnetically decoupled case) has been reported elsewhere [14].

Neutron diffraction and reflectivity measurements were carried out at the NIST Center for Neutron Research (NCNR) in Gaithersburg (USA). A triple-axis spectrometer (neutron wavelength $\lambda = 2.35$ Å) was set to the elastic mode of operation for the diffractometry experiments. Fig. 2(a) shows a diffraction scan with Q_z parallel to the SL [001] growth direction for sample III in zero magnetic field. Measurements above and below the Curie temperature $T_C = 18.5 \pm 0.5$ K (22 K and 4.3 K, respectively) were taken in order to separate the magnetic contribution from the structural part. The central peak ($Q_z = 0$) corresponds to the common (EuS and PbS) nuclear in-plane (020) Bragg reflection of the whole epitaxial structure grown on the KCl substrate. The smaller satellites visible only in the spectrum taken at 4.3 K are a signature of the AFM ordering between adjacent EuS layers. These peaks occur at $Q_z = \pm 0.038$ Å⁻¹, which is about $\pm 2\pi/2d$ where d is the bilayer repeat thickness of the SL ($d = 83$ Å for this sample). The expected positions of the first-order structural (nuclear) SL satellites are at $Q_z = \pm 0.076$ Å⁻¹. They are not visible in the scans due to the combined effect of the superlattice chemical structure factor, which has minima in the vicinity of $Q_z \approx \pm 0.07$ Å⁻¹, and considerably smaller nuclear scattering length density

(SLD) contrast between EuS and PbS than the magnetic SLD contrast. Similar arguments can be applied for the reflectometry measurements described below. The pure magnetic contribution to the scattering as shown in Fig. 2(b) is obtained by taking the difference of the two spectra in Fig. 2(a). The absence of any magnetic scattering at the central peak position and the presence of the satellites exactly halfway between the central peak and the expected first-order nuclear peak are clear evidence of AFM interlayer correlations in this EuS/PbS system.

The conclusion from the diffraction experiments is further corroborated by the results of the reflectometry studies. A reflectometer operating on the NCNR NG-1 cold neutron guide was employed to get the neutron reflectivity spectra. Due to the longer neutron wavelength ($\lambda = 4.75 \text{ \AA}$), the Q -resolution in the reflectivity measurements was considerably better than in the diffraction experiments. Fig. 3 shows the reflectivity profiles obtained for samples I and III at 4.3 K. In zero applied magnetic field, pronounced peaks at the Q_z position corresponding to twice the chemical SL periodicity were observed in both samples. These maxima are again clear indication of the AFM alignment of the magnetizations in successive EuS layers. To confirm the magnetic origin of these peaks, reflectivity spectra were also taken with an in-plane magnetic field. Application of a *sufficiently strong*, external magnetic field results in full parallel alignment of the ferromagnetic EuS layers; thus the AFM peak disappears, while the intensity of the FM peak at the structural position increases (Fig. 3). Details of the AFM peak decay with applied magnetic field are discussed below.

Fig. 4 shows the field dependence of the magnetization taken by a SQUID magnetometer with the in-plane field applied along the crystallographic [100] direction at 5K. The magnetic hysteresis loop for sample I shows a considerably harder magnetic behaviour than for sample III, indicating the interlayer coupling is stronger with the thinner PbS spacer. The lower remanence of Sample I — 7% compared to 62% of Sample III — clearly demonstrates that the coupling is *antiferromagnetic*. For sample II with intermediate spacer thicknesses, a step-like behavior is observed in the magnetization loop, which is shown in the lower-right inset of Fig. 4. The step-like behavior is a manifestation of the abrupt transition from one stable magnetic arrangement of the EuS layers to another. The upper-left inset shows an anomalous temperature dependence of the same sample ($d_{\text{PbS}} = 10 \text{ \AA}$). The decrease of the net magnetization with decreasing temperatures, observed for fields below 100 G, indicates that AFM coupling becomes stronger at low temperatures. For fields higher than 100 G, the temperature behavior of the magnetization starts resembling that typically seen in ferromagnetic systems. This is due to the coupling being too weak to overcome the applied field strength for all temperatures down to 5K. The measurements taken along the [110] crystallographic direction show essentially the same field and temperature dependence for all the samples used in this study.

The results of the field dependence studies of the AFM peak in the neutron reflectivity spectrum are shown in Fig. 5 for all three samples. The measurement procedure starts with the samples in zero magnetic field. The field is gradually increased until the AFM peak disappears, and then is decreased back to zero. All samples show initially a strong AFM peak before the application of the magnetic field. To erase entirely the AFM peak, a considerably larger fields are needed for sample I ($\sim 700 \text{ G}$) and sample II ($\sim 200 \text{ G}$) than for sample III ($\sim 75 \text{ G}$). The AFM peak for sample I and sample II is *recoverable*. The removal of the external field leads to the restoration of the AFM coupled state. The AFM peak of sample III is *not* recoverable. The sample remains in the *ferromagnetic* configuration after the removal of the external field. The irreversible destructive effect of the magnetic field on the AFM reflectivity peak is consistent with the fact that there are no traces of AFM coupling in the magnetic loop measurements for sample III. This suggests that the AFM coupling strength in sample

III, with the thickest spacer, is much weaker than in the sample I or II. It is also weaker than the anisotropy (domain pinning) fields in sample III that lock the FM spin configuration after removal of the external magnetic field. Similar behavior of the AFM peak in external magnetic field has been previously observed in Fe/Nb multilayers [15].

As noted, AFM coupling in all-semiconductor SL structures has not been predicted by previous theoretical models. In the case of layers exhibiting a domain structure with small enough average domain size ($1\mu\text{m}$ or less), the dipolar coupling, proposed in [16] for metallic structures, may become sizable. A characteristic feature of this coupling is the relatively weak dependence of its strength on the spacer thickness. The mean domain size can be evaluated from the width of transverse scans (wavevector transfer component parallel to the layers surface) through the magnetic superlattice Bragg peaks. In these scans performed for the sample I, a narrow, specular peak is observed, its width and shape being almost identical as that seen in the corresponding X-ray transverse scan. Thus the existing broadening beyond the instrumental resolution may be attributed to interface roughness and other structural imperfections and not to the magnetic domain scattering. Even if we attributed the total FWHM of this peak to domain scattering, it would set a lower limit on domain size of $\sim 3\mu\text{m}$. The dipolar coupling strength resulting from domains of this size with a 30 \AA EuS layer thickness is lower than 80 G (see formula (9) in [16]). Hence, the mechanism might only contribute for spacer thicknesses larger than in the presented samples. Traces of the interlayer coupling, slowly decreasing with the spacer thickness, indeed observed in the neutronographic spectra for SLs up to $d_{\text{PbS}} = 90\text{ \AA}$, can be perhaps attributed to the dipolar mechanism. However, the dipolar forces cannot explain the behavior for $d_{\text{PbS}} < 25\text{ \AA}$, where the data show a rapid increase of the coupling strength with decreasing PbS thickness ($\sim 700\text{ G}$ for sample I), clearly suggesting that another stronger AFM interaction takes over.

In search for a mechanism that could explain that stronger interlayer interaction, we analyzed the sensitivity of the total energy of valence electrons to the magnetic structure of a perfect $(\text{EuS})_m/(\text{PbS})_n(001)$ SL, where m and n are the numbers of EuS and PbS monolayers respectively (the monolayer thickness of both constituents is $\approx 3\text{ \AA}$). Specifically, we calculated the difference between the total electron energies of SLs with parallel and antiparallel spin directions in consecutive EuS layers. This difference is a measure of the magnetic interlayer coupling. We used an empirical tight-binding method, which, although being a one-electron method, should still describe adequately the small spin-dependent changes in the total energy. The values of most tight-binding parameters are chosen so as to reproduce the essential features of the band structures of bulk EuS [17] and PbS [18], the remaining being estimated by Harrison scaling. Our calculations indicate that the AFM spin alignment in successive EuS layers leads to a lower energy of the SL system, in accord with experimental observations. The coupling energy results primarily from the Eu ions at the magnetic/non-magnetic interfaces. The calculated coupling strength decreases with the thickness of the non-magnetic spacer roughly like 2^{-n} . This is in a very good agreement with the data presented in Fig. 5, which allow to estimate the strength of the coupling, from the value of magnetic field erasing the AFM neutron reflectivity peak (saturation field). A rough estimate of the magnitude of coupling strength can be made using the formula $J_1 = M_s B t / 4$ where M_s is the saturation magnetization, and t the thickness of an EuS layer [15]. As can be seen from the Fig. 5 these fields are $\sim 700\text{ G}$, $\sim 350\text{ G}$ and $\sim 200\text{ G}$ for $n=1, 2$ and 3 respectively. The first two values were deduced from the two slopes for the sample I visible in Fig. 5. As 4.5 \AA spacer is about 1.5 monolayers thick, the sample I may be considered as a mixture of two superlattices with $n = 1$ and 2 . Theoretically calculated values of J_1 for the *perfect* SL with $n=1, 2$ and $3 - 0.77, 0.33$, and 0.18 mJ/m^2 , respectively – although follow the same PbS spacer thickness dependence are about an order of magnitude higher than the experimental values estimated from the

saturation fields using the above formula (0.063, 0.031, and 0.019 mJ/m² respectively). One of the possible reasons for the latter discrepancy may be interfacial roughness and interdiffusion. Substantial reduction of the coupling strength in metallic multilayers due to the alloying effects in the interfacial regions have previously been reported [19]. The full, detailed description of the above theoretical calculations can be found in [20].

In summary, we have presented the first conclusive experimental evidence, based on neutron diffraction, neutron reflectivity, and magnetization measurements, for the existence of antiferromagnetic interlayer exchange coupling in a purely semiconductor, ferromagnetic/nonmagnetic epitaxial system with negligible carrier concentration. We have also shown that the experimentally observed sign, strength and range of the interaction may be well accounted for by band structure effects sensitive to the magnetic configuration of the multilayer.

* * *

Acknowledgments: Work supported by projects: NATO PST.CLG 975228, NSF DMR-9972586, KBN 2 P03B 007 16, and KBN 2 P03B 154 18.

REFERENCES

- [1] PRINZ G. A., *Science*, **282** (1998) 1660.
- [2] BRUNO P., *Phys. Rev. B*, **52** (1995) 411.
- [3] JONES B. A., *IBM J. of Res. and Dev.*, **42** (1998) 25.
- [4] STRIJKERS G. J., KOHLHEPP J. T., SWAGTEN H. J. M. and DE JONGE W. J. M., *Phys. Rev. B*, **60** (1999) 9583; *Phys. Rev. Lett.*, **84** (2000) 1812.
- [5] KĘPA H., GOLDMAN K. I., GIEBULTOWICZ T. M., MAJKRZAK C. F., SPRINGHOLZ G., KRENN H., HOLL S., SCHINAGL F. and BAUER G., *Physica E*, **2** (1998) 399.
- [6] RHYNE J. J., LIN J., FURDYNA J. K. and GIEBULTOWICZ T. M., *J. Magn. & Magn. Mater.*, **177-181** (1998) 1195.
- [7] NUNEZ V., GIEBULTOWICZ T. M., FASCHINGER W., BAUER G., SITTE H., and FURDYNA J. K., *J. Magn. & Magn. Mater.*, **140-144** (1995) 633.
- [8] CHIBA D., AKIBA N., MATSUKURA F., OHNO Y. and OHNO H., *Appl. Phys. Lett.*, **77** (2000) 1873.
- [9] OHNO H., *Science*, **281** (1998) 951.
- [10] DIETL T., OHNO H., MATSUKURA F., CIBERT J. and FERRAND D., *Science*, **287** (2000) 1019.
- [11] SHEVCHENKO P., ŚWIĘRKOWSKI L. and OITMAA J., *J. Magn. & Magn. Mater.*, **177-181** (1998) 1168.
- [12] DUGAEV V. K., LITVINOV V. I., DOBROWOLSKI W. and STORY T., *Solid State Commun.*, **110** (1999) 351.
- [13] BLINOWSKI J. and KACMAN P., *Acta Phys. Pol. A*, **92** (1997) 719.
- [14] STACHOW-WÓJCIK A., STORY T., DOBROWOLSKI W., ARCISZEWSKA M., GAŁĄZKA R. R., KREIJVELD M. W., SWÜSTE C. H. W., SWAGTEN H. J. M., DE JONGE W. J. M., TWARDOWSKI A., and SIPATOV A. YU., *Phys. Rev. B*, **60** (1999) 15220.
- [15] REHM CH., NAGENGAST D., KLOSE F., MALETTA H. and WEIDINGER A., *Europhys. Lett.*, **38** (1997) 61.
- [16] BORCHERS J. A., GEHRING P. M., ERWIN R. W., ANKNER J. F., MAJKRZAK C. F., HYLTON T. L., COFFEY K. R., PARKER M. A. and HOWARD J. K., *Phys. Rev. B*, **54** (1996) 9870.
- [17] CHO S. J., *Phys. Rev. B*, **1** (1970) 4589.
- [18] SU-HUAI WEI and ZUNGER A., *Phys. Rev. B*, **55** (1997) 13605.
- [19] BRUNO P., *Magnetische Schichtsysteme*, edited by P. H. DEDERICHS and P. GRÜNBERG (Forschungszentrum, Jülich) 1999.
- [20] BLINOWSKI J. and KACMAN P., *Phys. Rev. B*, **64** (2001) 045302.

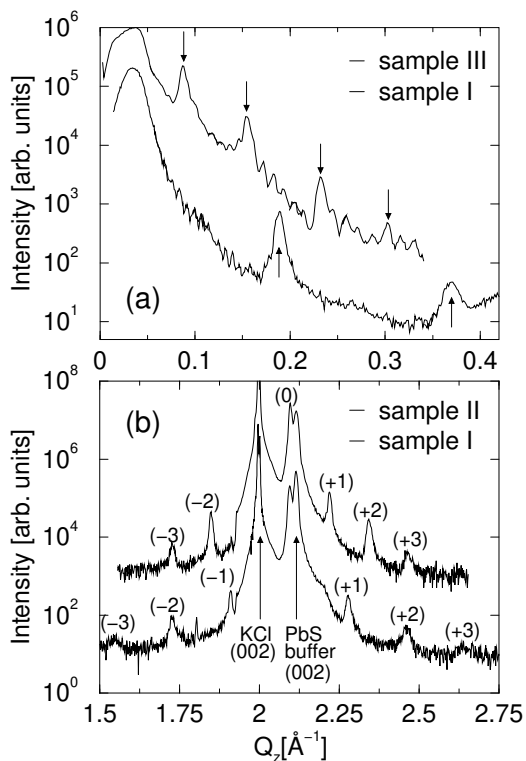


Fig. 1

Fig. 1 – (a) X-ray reflectivity profiles taken for the samples III and I. Total reflection regions and a number of superlattice Bragg peaks (marked by arrows) are clearly visible. (b) Wide angle diffraction spectra taken about (002) reciprocal lattice point for the samples II and I. Apart from strong (002) Bragg reflections from the KCl substrate and PbS buffer layer, large number of smaller SL satellites is also present proving the high structural quality of the investigated samples.

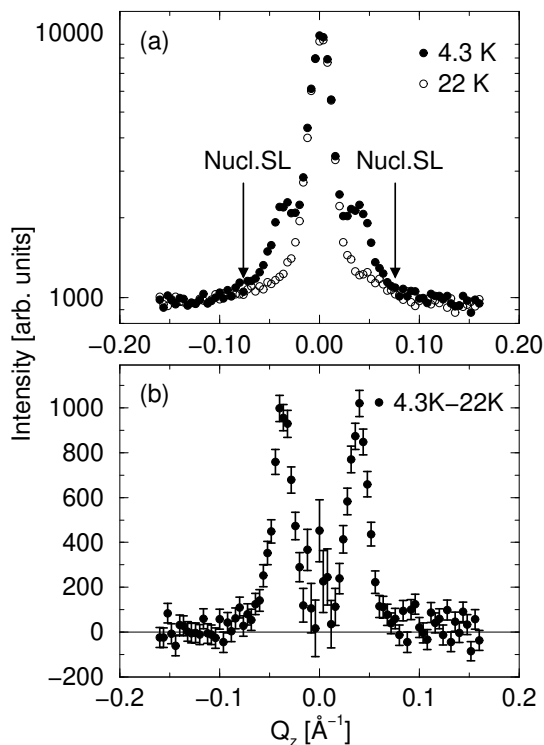


Fig. 2

Fig. 2 – (a) Neutron diffraction scan with Q_z parallel to the SL [001] growth direction about the reciprocal lattice point $(0, 2.14, Q_z)$ above and below T_C for sample III. The arrows in (a) shows the expected positions of the first order nuclear SL satellites. (b) The purely magnetic contribution is found by taking the difference between the two spectra in (a).

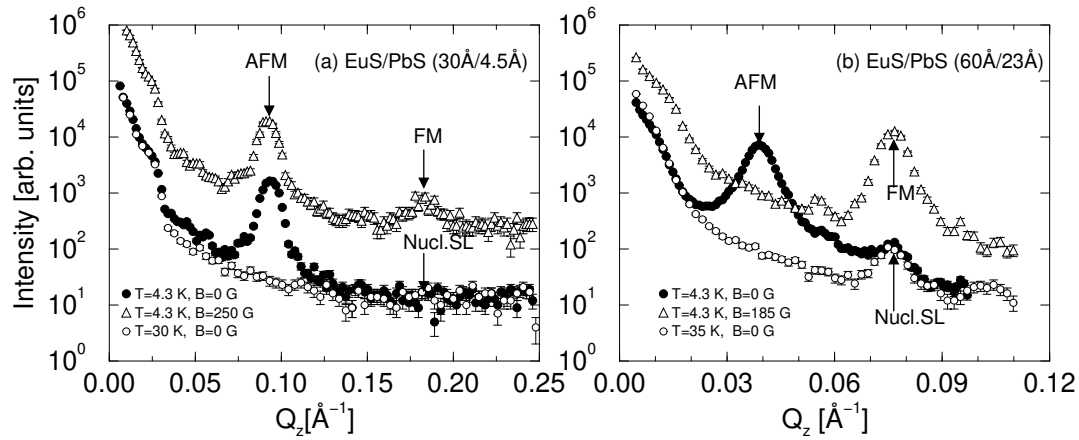


Fig. 3 – Neutron reflectivity spectra taken at 4.3 K in zero field and in 250 G (below the saturation value) for sample I (a), and in zero and 185 G (well above the saturation value) for sample III (b). For sample I the applied intermediary field strength 250 G reduces the AFM peak intensity only by half, emerging FM peak is also visible. Data taken at 35 and 30 K (above T_C) show the nonmagnetic contributions to the scattering. The reflectivity curves measured in magnetic fields are shifted one order of magnitude up for greater clarity.

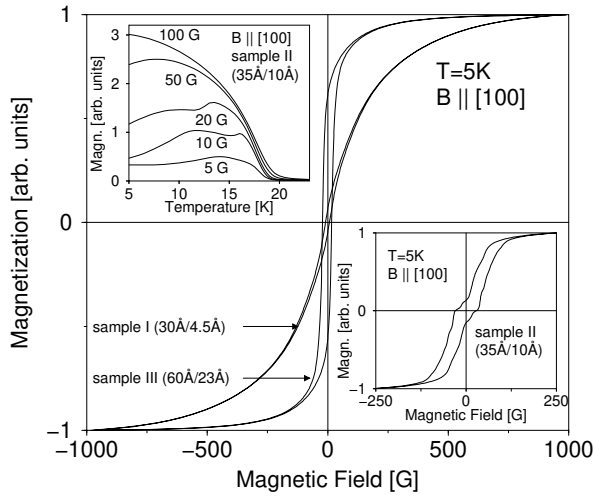


Fig. 4

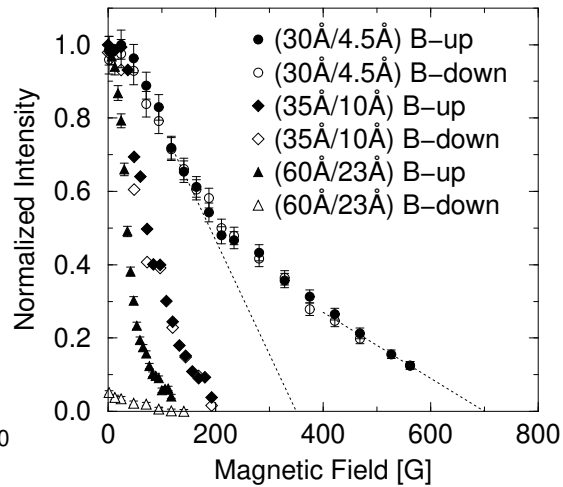


Fig. 5

Fig. 4 – Field dependence of the magnetization of sample I and III along the crystallographic [100] direction at 5 K is studied using a cryogenic superconducting quantum interference device (SQUID) magnetometer. The lower-right and upper-left insets show the magnetization behaviour versus field and temperature respectively of the sample II.

Fig. 5 – Magnetic field dependence of the AFM reflectivity peak intensity for samples I, II, and III. Closed and open symbols represent the data taken with increasing and decreasing fields respectively. The two slopes visible for the sample I, indicated by the dotted lines, show the behavior of two regions in the specimen with the 1 and 2 monolayer thick PbS spacer (see text).